Progress In Electromagnetics Research, PIER 60, 311–333, 2006

CHARACTERIZATION OF THE OPEN-ENDED COAXIAL PROBE USED FOR NEAR-FIELD MEASUREMENTS IN EMC APPLICATIONS

D. Baudry, A. Louis, and B. Mazari

IRSEEM
Technopôle du Madrillet, Avenue Galilée BP 10024
76801 Saint Etienne du Rouvray Cedex, France

Abstract—A completely automatically near-field mapping system is developed within IRSEEM (Research Institute for Electronic Embedded Systems) in order to determine electromagnetic field radiated by electronic systems. This test bench uses a 3D positioning system of the probe to make accurate measurements. The main element of this measurement tool is the probe. This paper presents a characterization of the open-ended coaxial probe which is used to measure the normal component of the electric field.

1. INTRODUCTION

Nowadays, electronic systems are integrating more and more functionalities in a confined volume; however, some components generate electromagnetic interference (EMI) problems. The complexity of these devices can reduce the efficiency of each function. The knowledge of the electromagnetic environment is therefore essential. Traditional measurement systems which use network analyzers or classical simulation tools do not enable us to determine the electromagnetic near field which is close to complex and especially active devices. It is therefore necessary to use near-field measurements to characterize EMI problems.

The use of Near-field techniques in EMC applications increases rapidly. These techniques are used to characterize a complete system [1] but also to locate the emission sources inside a component [2, 3]. To reach this objective, the near-field test bench and especially the performances of the used probes must be well known.

IRSEEM (Research Institute for Electronic Embedded Systems) is developing a near-field test bench to carry out these measurements;

this equipment collects the electromagnetic field close to devices of various sizes. Different passive planar circuits [4] and active devices [5] validated the ability of the bench for measuring relative amplitude of all the electromagnetic field components. Effective measurements of radiated emissions need the calibration of the probe. An understanding of coupling mechanism is necessary for choosing an appropriate calibration method for near field measurement probe. This paper presents a characterization of the coaxial probe and a calibration technique [6]. In the last part, absolute amplitude and phase measurements of a hybrid junction are presented.

2. EXPERIMENTAL SETUP

The system is based on a direct measurement method [7, 8]. The probe is connected to a spectrum analyzer and is mounted on a five-axis robot. A computer monitors the probe displacement over the device under test (DUT) and acquires data provided by the spectrum analyzer (Fig. 1). The maximum scanning area is $200\,\mathrm{cm}(x) * 100\,\mathrm{cm}(y) * 60\,\mathrm{cm}(z)$ with a mechanical resolution by 10μm in the three directions (x, y and z) and $0.009°$ for the two rotations.

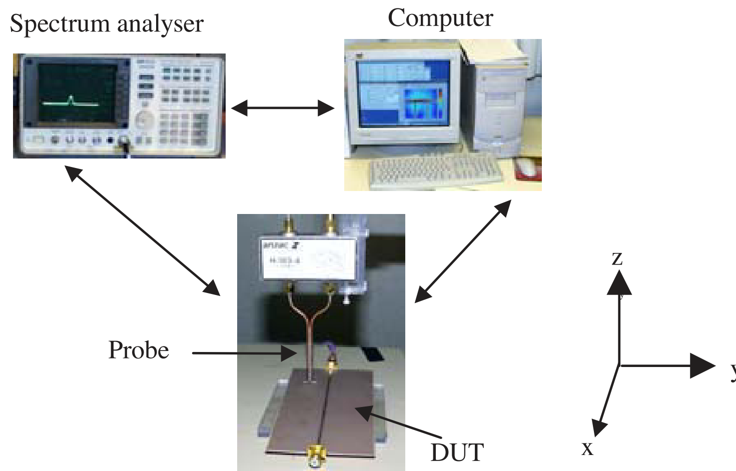

Figure 1. Synoptic of the test bench.

The probe must be close to the surface of the components in order to ensure a good resolution of measurements. A 3D positioning system based on relief measurements allows maintaining a constant distance between the probe and the device. The method used to acquire the

relief model of objects is based on laser triangulation. The object is illuminated from one direction with a laser line projector and viewed with the camera from another one. Laser and camera are held on the robot (Fig. 2). Translating the positioning system along the x axis of the robot enables to acquire the relief model of the device under test. Camera-provided Z data are recorded on a computer and converted into probe coordinates. Finally, these data are used to position the probe over the device under test during electromagnetic measurements.

Figure 2. 3D positioning system.

Measurements of all the components of the electromagnetic field are achieved with three different probes (Fig. 3). The first probe [9] is used to measure the three components of the magnetic field. It consists of a small loop made with inner conductor of two adjacent coaxial cables. The probe measures the magnetic field that is perpendicular to the loop. The three components of the magnetic field are obtained by rotating the probe with an angle of 90° around the three x, y and z directions. The second probe is a balanced wire dipole that consists of two adjacent coaxial cables and a hybrid 180° junction to balance the dipole [10]. This dipole is used to measure the tangential components of the electric field (E_x and E_y). A spectrum analyzer measures the difference between the two signals of the junction output ports. E_x and E_y components of the electric field are measured by rotating the probe with an angle of 90° around z axes. The last probe (EPZ1) used to measure the normal component of the electric field (E_z) consists of a 50Ω open-end coaxial cable oriented in a parallel direction to this field. This probe has an inner conductor diameter of 500μm. Next

parts of this work are only focused on this last probe.

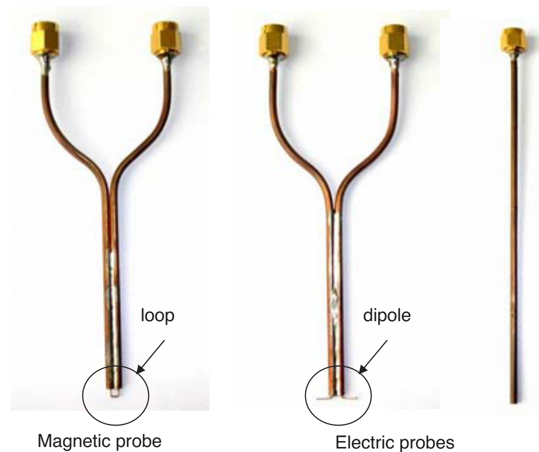

Figure 3. Magnetic and electric probes.

3. VALIDATION OF THE TEST BENCH

In order to validate the test bench, a simple passive circuit is measured and experimental results are compared with simulated ones. All simulations are made with Ansoft HFSS a commercial 3D electromagnetic simulator based on Finite Element Method (FEM). The sample circuit tested is a 50Ω micro-strip line at a frequency of 1 GHz. The line has a length of λ (wavelength of radiation). Substrate's thickness and relative permittivity are respectively 0.8 mm and 4.4. The measurements are implemented for three distances d between the probe and the DUT: 1, 2 and 5 mm. The micro-strip line is oriented along the x axis and the centre of the line is at $y = 0$ mm. Complete cartographies of the micro-strip line in short circuit and open circuit are presented on Fig. 4.

We can see that field's maximum is located on the center of the line as expected by the theory. Measurements show also the standing wave patterns with a period of $\lambda/2$ and a shift of $\lambda/4$ between short circuit and open circuit. The probe resolution enables detecting field minima on the edges of micro-strip line.

Next we compared experimental results with simulated ones. Results are presented Fig. 5 with measurement on the left side and simulation on the right side. In the absence of calibration, a translation factor is applied to simulation in order to put maxima at the same level. We can note a quite good accordance between measurement and

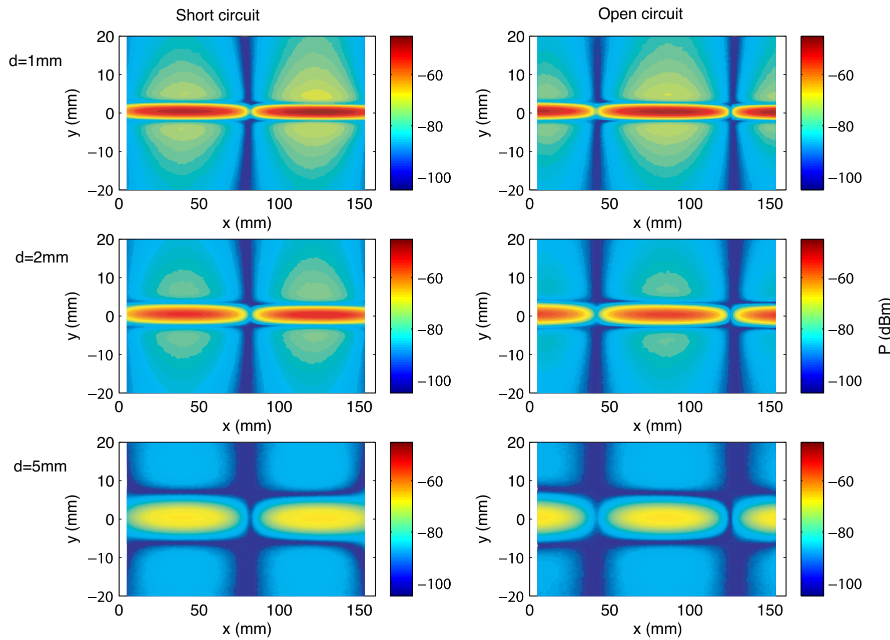

Figure 4. Measurement of normal electric field at selected height above micro-strip line.

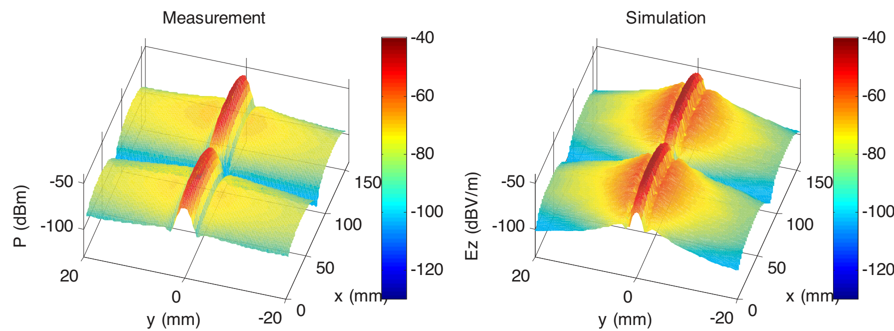

Figure 5. Mapping of the normal component of the electric field.

simulation. The main differences are secondary peaks not present on the measurement and a greater distance between minima.

This first measurement on a micro-strip line shows that the coaxial probe mainly detects the normal component of the electric field but differences exist between measurement and simulation. In a second

step, we make a parametric study of this probe to understand these differences and to characterize the probe.

4. STUDY OF THE OPEN-ENDED COAXIAL PROBE

4.1. Simulation of the Global System

We simulate the complete system probe and micro-strip line in order to verify that differences between measurement and simulation are due to the transfer function of the probe. The probe is moved during the simulation along a transverse line (y axis) and the transmitted power (S_{31}) is calculated between one port of the line and the port of the probe. For both simulation and measurement the micro-strip line is loaded by an impedance of 50Ω. The results we obtained are shown on Fig. 6. The simulation of the normal component of the electric field (E_z) is also plotted on this graph. The good accordance between measurement and simulation confirms that differences between measurement and theory are not due to outer disturbance of the test bench, but definitely to results of an electromagnetic field coupling with the outer conductor of the coaxial probe.

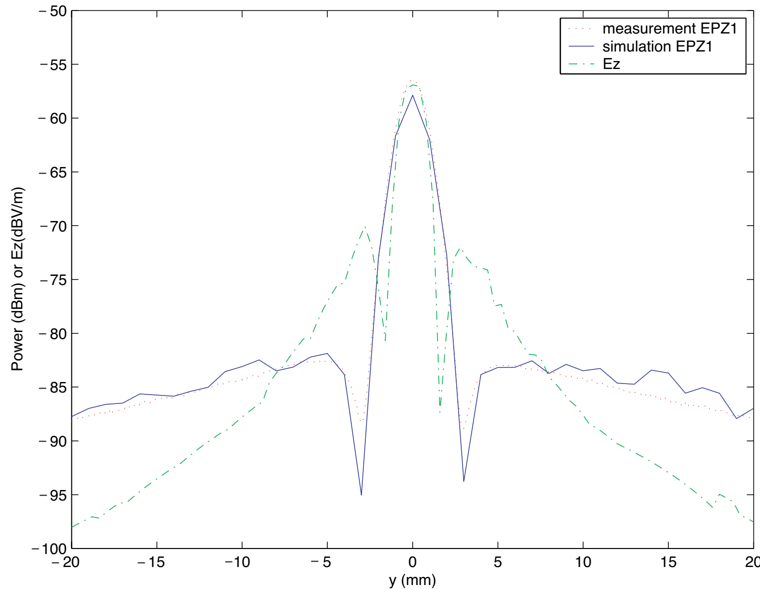

Figure 6. Measurement and simulation of a cross section at 1 mm over the micro-strip line.

4.2. Influent Parameters and Criteria of Comparison

The studied geometrical parameters of the coaxial probe are represented on Fig. 7. The length ℓ of the inner conductor, the diameter D of the probe and the size of the metallic plate composed these studied parameters. To characterize the probe we select different criteria: selectivity, spatial resolution, frequency bandwidth, induced perturbation and cross section measurement. The selectivity corresponds to the ability of the probe to separate the normal component of the electric field from the others electromagnetic components. The spatial resolution corresponds to the limit distance of separation of two sources. The induced perturbation explains the influences of the probe on the DUT performances. The last criterion called cross section allows to study coupling between the probe and the electromagnetic field. Measurements of cross section over micro-strip line are compared to simulations to evaluate these criteria.

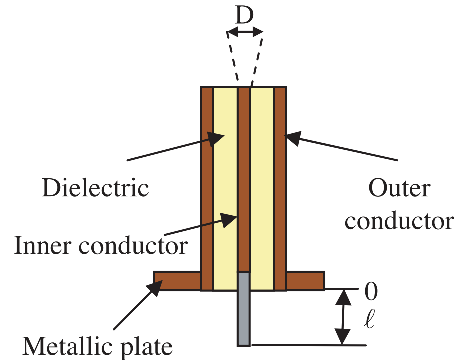

Figure 7. Studied parameters of the coaxial probe.

4.3. Influence of the Length of the Inner Conductor

In a first step, we implement a simulation of the coaxial probe in free space to study the selectivity of the probe. The study is carried out for two lengths of the inner conductor extent: 0 mm and 5 mm. The probe is stressed by an external plane wave with a polarisation angle φ at the frequency of 1 GHz (Fig. 8).

The plane wave is propagating perpendicularly to the probe axes with the incident electric field of 1 V/m. The expression of the electric field is given by Eq. (1).

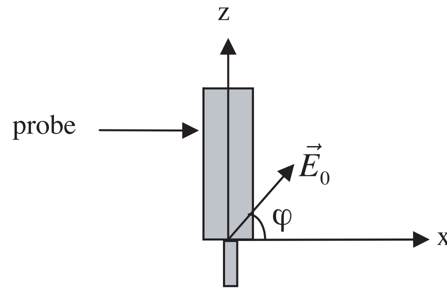

Figure 8. Illumination of EPZ1 probe with a plane wave.

$$\vec{E} = E_0 cos(\varphi) e^{-jky}\ \vec{u_x} + E_0 sin(\varphi) e^{-jky}\ \vec{u_z} \quad (1)$$

Output voltage (ΔV) calculated for angles varying from 0° to 90° are presented on Fig. 9. Curves sin(φ) are added to these graphs. Calculated tensions are well interpolated by sinusoidal functions. These simulations show that the output voltage delivered by the coaxial probe is proportional to the normal component (E_z) of the electric field for the two lengths of inner conductor.

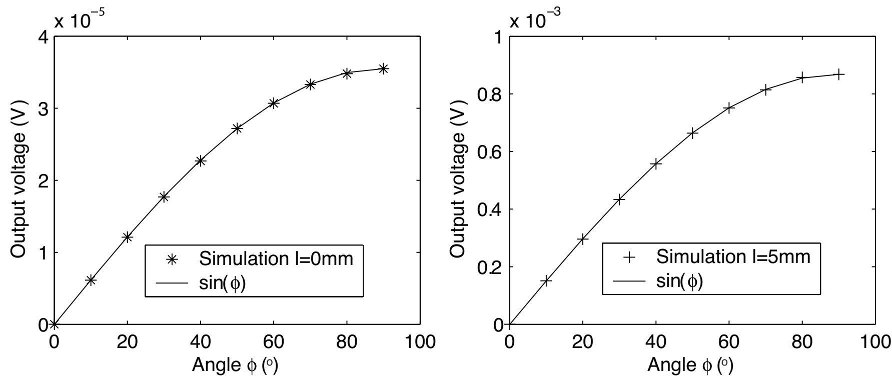

Figure 9. Simulations of output probe voltage for different polarization angle φ.

In a second stage we study the influence on measurements of the length ℓ of the inner conductor that exceeds the external conductor. Simulations of a cross section at 1 mm over the micro-strip line are carried out for different lengths of the inner conductor. This length varies from 0 mm (no extension of the inner conductor) up to 5 mm.

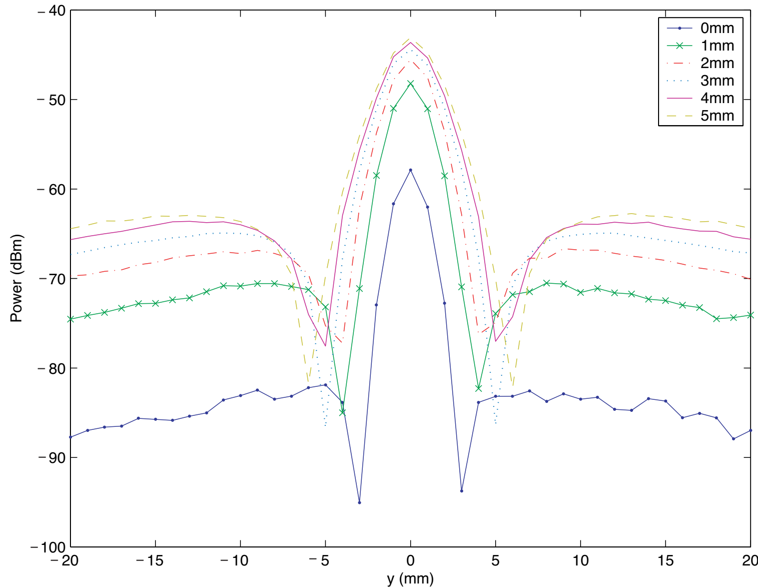

Figure 10. Influence of the length of the center conductor.

Results presented on Fig. 10 show that a rise of the inner conductor length increases the sensitivity of the probe but also increases the distance between minima (corresponding to maxima of E_y component). This is probably due to the integration of the normal component of the electric field on the length of the inner conductor.

To confirm these first results, we made a simulation of the coaxial probe in free space. The probe is illuminated with a plane wave described by Eq. (1) with an angle φ of 90°. Simulations are implemented at 1 GHz for inner conductor lengths varying from −5 mm to 5 mm by step of 1 mm. Output voltage delivered by the probe is plotted on Fig. 11. We can note a linear variation of the output voltage for inner conductor lengths in the range 0–5 mm. For negative values corresponding to an extent of the outer conductor, the output voltage is close to zero as the outer conductor acts as a screen. These results confirm the precedent ones, i.e., the sensitivity is proportional to the inner conductor length.

4.4. Influence of the Diameter of the Probe

In this part we study the influence of the diameter of the probe on three characteristics: the sensitivity, the spatial resolution and the frequency

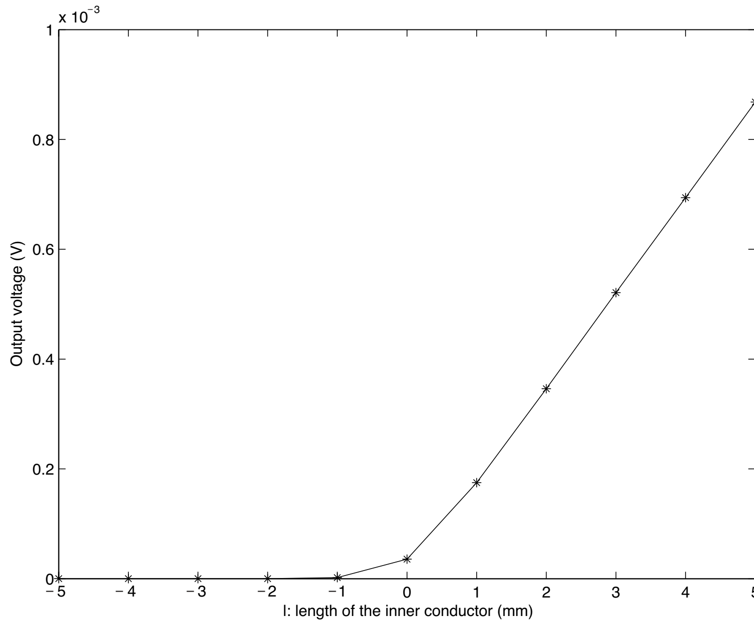

Figure 11. Simulations of output probe voltage for different lengths of the inner conductor.

bandwidth. The output voltage delivered by the probe for inner conductor diameter varying between 100μm and 2 mm is calculated to study the influence on the sensitivity. For these simulations, the probe is placed over the centre of the micro-strip line. Corresponding results are presented on Fig. 12. These results show that the sensitivity of the probe increases when the diameter of the probe grows which corresponds to a bigger integration's surface. The second information delivered by these simulations is the non-linear variation between the output voltage and the surface S of the inner conductor. While using the capacitive model which is classically used to describe these probes, it must have a linear variation between the output voltage or current and the surface S : $i = j\omega\epsilon_0 E_z S$ [8]. Capacitive model does not take into account coupling with external conductor. To validate this model, we made a simulation of the probe inserted in a rectangular waveguide. To avoid coupling with the external conductor, the probe levels the wall of the waveguide. Results are presented on Fig. 13. The output voltage is perfectly interpolated by a line confirming the capacitive model. This configuration allows avoiding parasitic coupling with the external conductor.

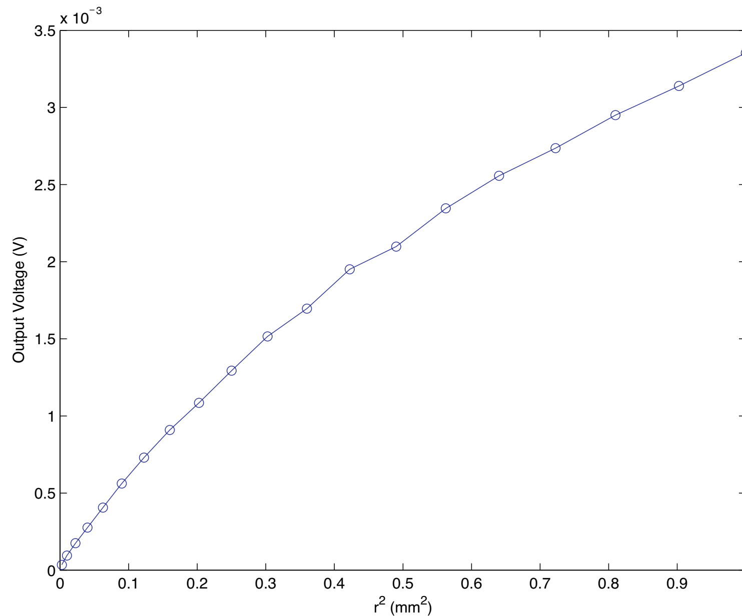

Figure 12. Output voltage for different diameters of probe in microstrip line configuration.

To study the influence of the probe's diameter on the spatial resolution, a new probe called EPZ2 is implemented. This probe has an inner conductor diameter of 300μm and a characteristic impedance of 50Ω. The DUT used for testing this parameter is a section of coupled lines connected to a generator and a 50Ω load. Each track has a width of 300μm. The gap is 300μm between the tracks. This configuration allows getting a maximum on each track for the normal component of the electric field if the cross section is close to the surface. To determine the correct distance, electromagnetic simulations are achieved. Obtained results show that the distance must be lower than 400μm to separate the two maxima. Next, cross sections are made at 1 GHz and 8 GHz for the two probes with a distance of 200μm between the probe and the DUT. Corresponding results are plotted on Fig. 14. The step between two acquisition points is 100μm.

For EPZ1 probe, the curves present a shoulder at the peaks level but do not allow to distinct the two maxima generated by the coupled lines. The distance of 600μm corresponds to the limit of resolution for this probe. For EPZ2 probe, the curves present two maxima with a local minimum between these maxima lower than 2.5 dB. These

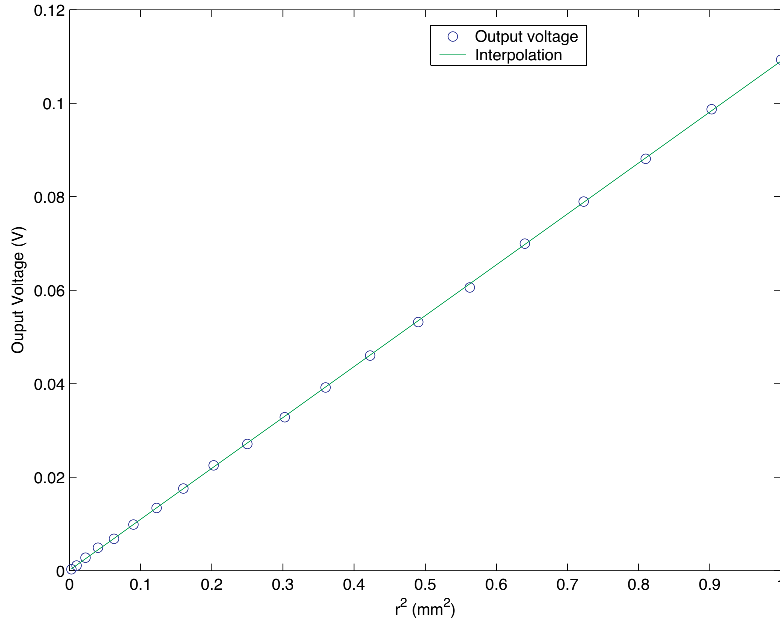

Figure 13. Output voltage for different diameters of probe in rectangular waveguide configuration.

experiments show that EPZ2 probe has a spatial resolution lower than 600μm. The frequency has no influence on the spatial resolution.

The last studied criterion is the frequency bandwidth of the probe. EPZ probe corresponds to a coaxial waveguide. The first propagation mode is TEM (Transverse ElectroMagnetic) which has a zero frequency cutoff. The upper frequency depends of the apparition of high order modes which is the TE_{11} mode for this particular waveguide. This frequency can be approximated with Eq. (2) [11] and values for EPZ1 and EPZ2 probe are given in Table 1. The frequency bandwidth of the probes is superior to the test bench bandwidth which is 10 kHz–10 GHz. The main limitation of the coaxial probe is the sensitivity of the probe for lower frequency due to the capacitive coupling.

$$f_{cTE_{11}} \approx \frac{c}{\pi(a+b)\sqrt{\epsilon_r}} \tag{2}$$

4.5. Addition of a Small Metallic Plate

Dahele et al. [12] show that the addition of a metal plate to the probe improves the accordance between measurement and theory by

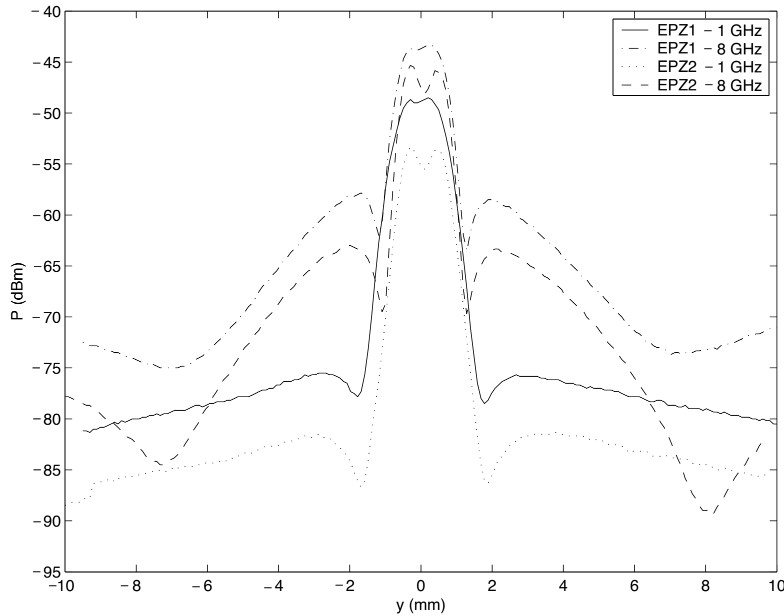

Figure 14. Cross section at 1 GHz and 8 GHz for EPZ1 and EPZ2 probe.

Table 1. TE_{11} Frequency cutoff for EPZ1 and EPZ2 probe.

Probe	Inner conductor radius a (μm)	Outer conductor radius b (μm)	TE_{11} frequency cutoff (GHz)
EPZ1	255	840	60
EPZ2	155	470	107

reducing spurious coupling. However the presence of this ground plane transforms the open structure in a shielded one and does not allow the knowledge of the electric field radiated by the open structure. We made a new coaxial probe (EPZ1_MP) terminated in a small perpendicular ground plane (Fig. 7) in order to minimize this problem. The ground plane is a 1cm by 1cm metal plate in which the open-ended coaxial cable is inserted. The measurement we obtained with EPZ1_MP probe on the micro-strip line is shown in Fig. 15 and compared to EPZ1 probe and theory.

Profile obtained with the EPZ1_MP probe shows a very good

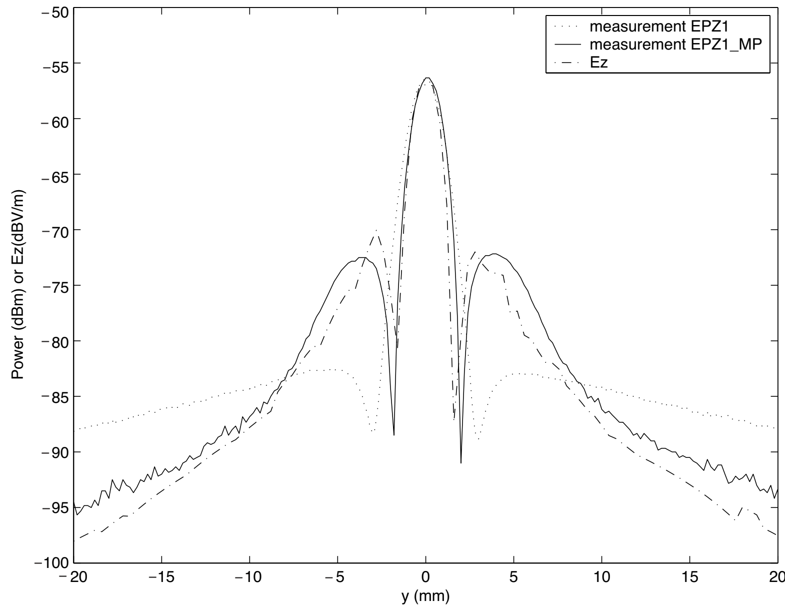

Figure 15. Cross section at 1 mm over the micro-strip line for EPZ1, EPZ1_MP probe and theory.

accordance with the theory. The small metallic plate added to the coaxial probe reduces coupling with the outer conductor. As the electromagnetic field radiated by the micro-strip line decreases rapidly we can assume that most of the coupling is due to a small portion of the extremity of the probe's outer conductor. The presence of the metallic plate allows avoiding this phenomenon. The repartition of the current distribution on the outer conductor (Fig. 16) confirms this explanation. On the extremity of the probe, current distribution is lower for the probe with a metallic plate.

To study the influences of the metallic plate, a simulation is made with dimensions varying between 0 to 20 mm. Probe transmitted power (Fig. 17) and transmission coefficient of the line (Fig. 18) are calculated. These results show that when the size of the plate is greater than 12 mm, secondary peaks are flattened and the transmission is disturbed by the probe. These phenomena probably result from parasitic coupling between the line and the plate, probe and micro-strip line forming an equivalent strip-line structure.

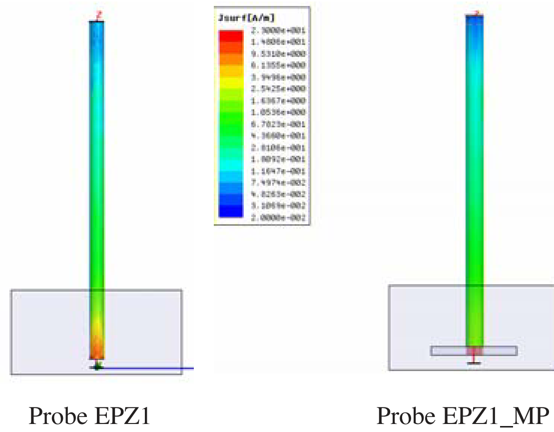

Figure 16. Current distribution on the external conductor.

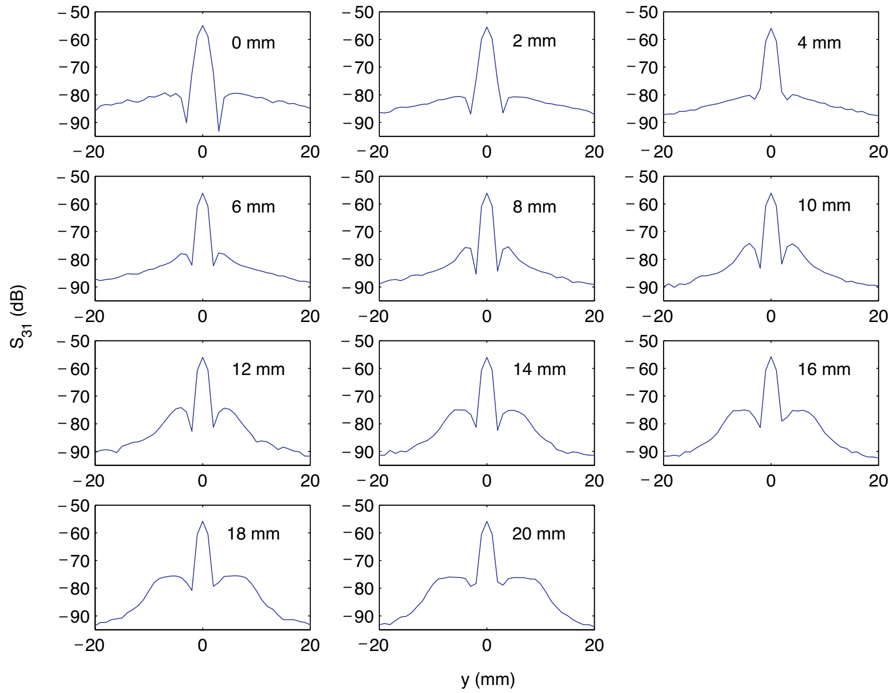

Figure 17. Influences of the plate on transferred power (S_{31}).

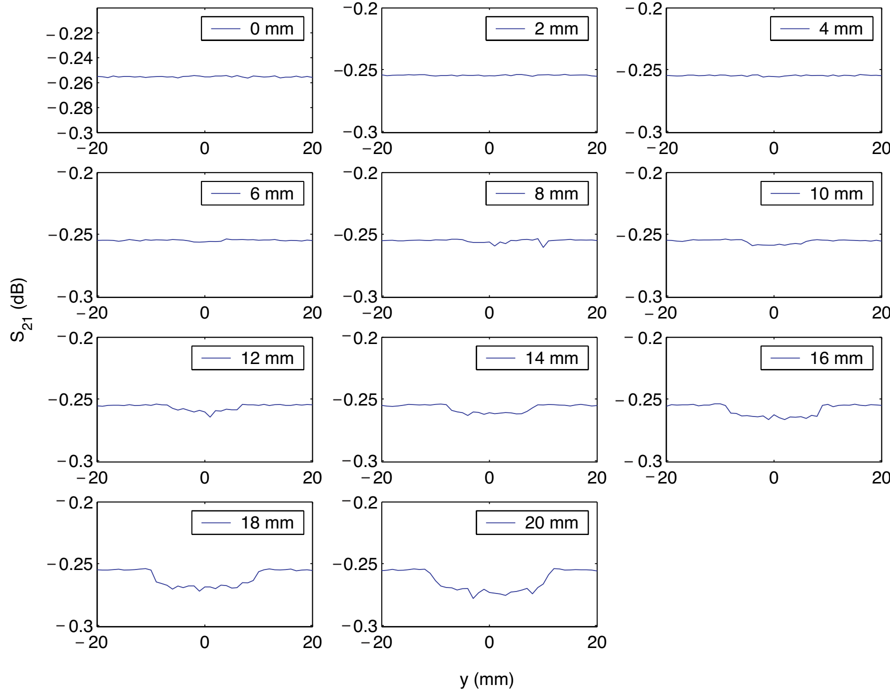

Figure 18. Influences of the plate on transmission coefficient (S_{21}).

5. CALIBRATION OF PROBES

Due to previous results a calibration in a well-known field (calculated or measured with calibrated probe) like in TEM cell or waveguide can give various results according to the insertion length of the probe in the field. So we choose a configuration where the field decreases rapidly along the probe. To calibrate the probe, a wire over ground plane (Fig. 19) is used instead of a micro-strip line because an analytical expression of the field can be calculated.

Analytical expressions of the transverse electric and magnetic field components (E_y in Eq. (3), E_z in Eq. (4), H_y and H_z in Eq. (5)) are obtained by electrostatic calculation with use of image theory [12, 13]. In Eq. (6), P is the incident power and $Z_c = 50\Omega$ the characteristic impedance of the transmission line.

$$E_y = 8K\left(\frac{yzn}{(y^2+(z+n)^2)*(y^2+(z-n)^2)}\right) \tag{3}$$

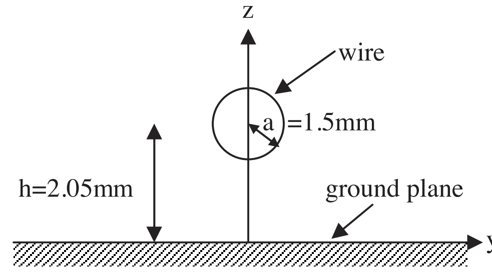

Figure 19. Wire over ground plane configuration.

$$E_z = 4K\left(\frac{n(y^2 - z^2 + n^2)}{(y^2 + (z+n)^2) * (y^2 + (z-n)^2)}\right) \tag{4}$$

$$H_y = -\frac{1}{\eta}E_z \text{ and } H_z = \frac{1}{\eta}E_y \text{ with } \eta = \sqrt{\frac{\mu_0}{\epsilon_0}} \tag{5}$$

$$\text{with } n = \sqrt{h^2 - a^2} \text{ and } K = \sqrt{2PZ_c}/\ln\left(\frac{h+n}{h-n}\right) \tag{6}$$

To validate these expressions, we make an electromagnetic simulation of the wire over ground plane at 1 GHz. Electric field obtained by electromagnetic simulation at 1 mm above the wire is compared to analytical one (Fig. 20). Results obtained by electromagnetic simulation are in perfect accordance with analytical fields.

The test set-up used to calibrate the probe is composed of the wire over ground plane loaded by 50Ω impedance. The line is connected to a generator delivering a power P. The probe (EPZ1 or EPZ1_MP) is connected to a spectrum analyzer and centered on the wire at 1 mm above. An antenna factor (Eq. (7)) is calculated for each probe over the frequency bandwidth (150 MHz–1.5 GHz) by using Eq. (4) and voltage measured by the spectrum analyzer.

$$AF_{dB}(f) = 20 * \log_{10}\left(|E_z|/V(f)\right) \tag{7}$$

The antenna factor calculated at 1 GHz is applied on previous measurements (Fig. 15) made with EPZ1 and EPZ1_MP probe at 1 mm over the micro-strip line and compared to the normal component of the electric field (Fig. 21). Electric field values obtained with EPZ1_MP probe are very close to theoretical field. For this probe, the antenna factor is equivalent to the translation factor applied on simulation. For EPZ1 probe, the antenna factor and the translation factor are different. These differences can be due to spurious coupling which are not taken into account in the antenna factor.

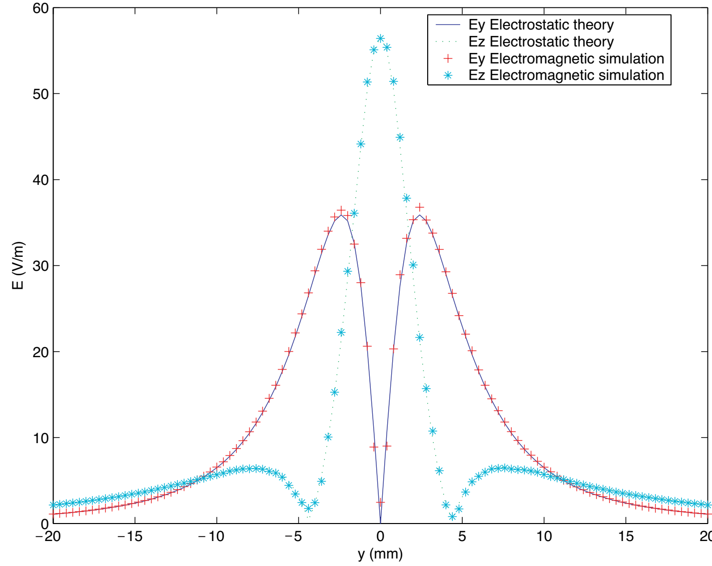

Figure 20. Comparison between analytical field and simulated field.

6. MEASUREMENT OF A QUADRATURE HYBRID JUNCTION

The test circuit is a quadrature hybrid junction (see Fig. 22). The coupler is implemented with micro-strip line on FR4 substrate ($\epsilon_r = 4.4$ and $h = 0.8\,\text{mm}$) material. The device is tested at 1 GHz. Port 1 is connected to the generator which delivers 0 dBm.

The S parameters matrix is given by Eq. (8). The DUT divides the entrance power at port 1 with an equal repartition on ports 2 and 3. A phase difference for output signals on ports 2 and 3 is equal to 90°. On an ideal coupler, there is no power on port 4.

$$[S] = \frac{1}{\sqrt{2}} \begin{bmatrix} 0 & j & 1 & 0 \\ j & 0 & 0 & 1 \\ 1 & 0 & 0 & j \\ 0 & 1 & j & 0 \end{bmatrix} \tag{8}$$

Amplitude measurements for EPZ1_MP (Fig. 23) are corrected with the antenna factor determined by calibration. Corresponding simulation is presented on Fig. 24.

For the normal component of the electric field, we can see that the field is maximum over the micro-strip line between port 1 and port 2 and between port 1 and port 3, while the field is less important on port

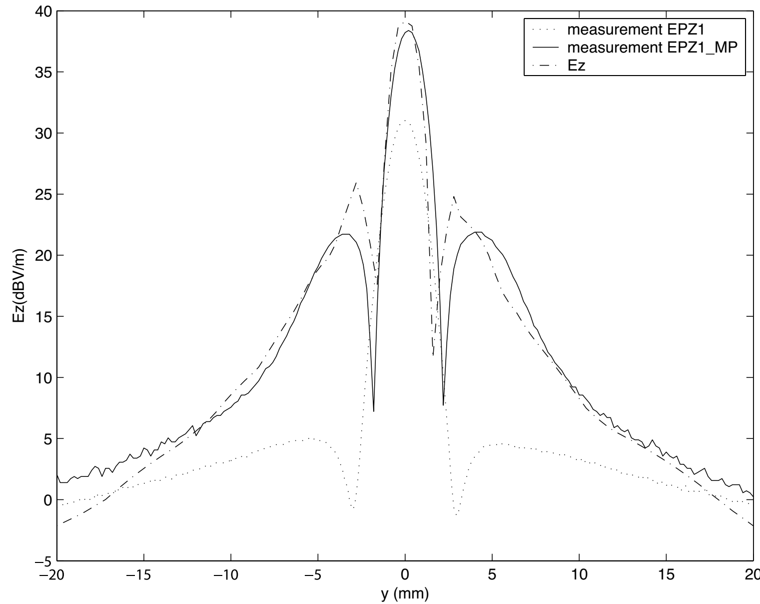

Figure 21. Measurements corrected with the antenna factor for EPZ1 and EPZ1_MP probe.

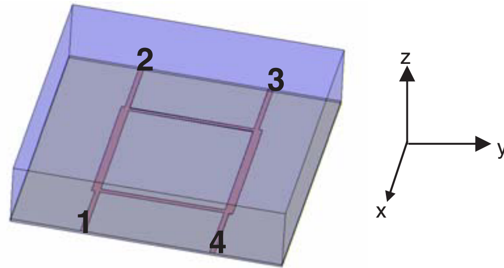

Figure 22. Device topology.

4. As expected by theory, transmission is maximum between port 1 and ports 2 and 3. Port 4 is isolated. We can also note a good accordance between simulations and measurements. Next, we implement the phase measurement of the DUT. Spectrum analyzer is replaced by a network analyzer and a low noise amplifier is used to compensate the lack of sensitivity. Resulting map is presented on Fig. 25 and a cross section along y axis close to ports 2 and 3 on Fig. 26. The graph corresponding to the cross section is corrected to avoid $\pm 2\pi$ jump between two points.

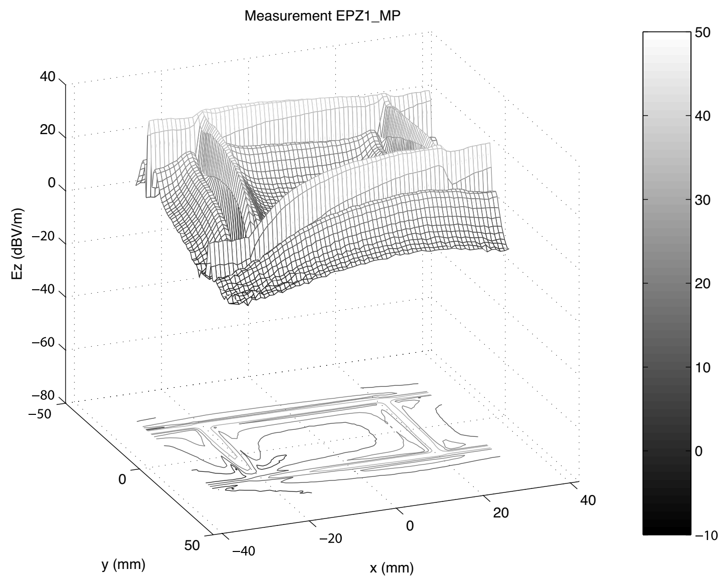

Figure 23. Measurement with EPZ1_MP of the normal (E_z) component of the electric field.

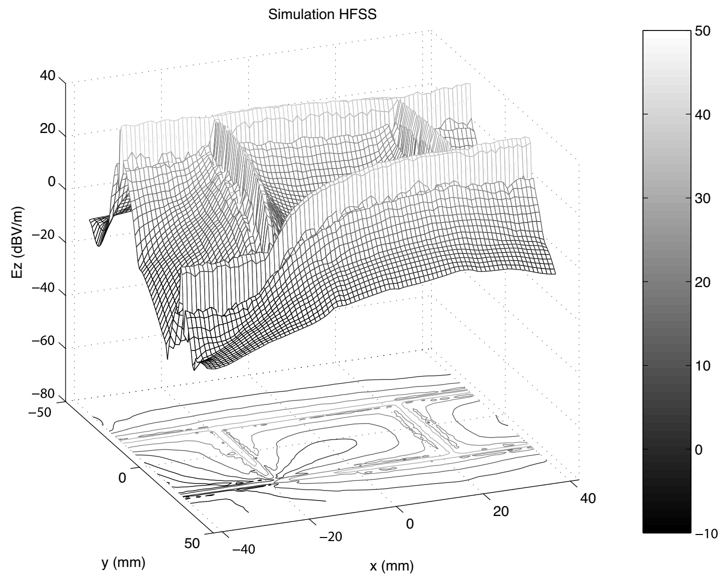

Figure 24. Simulation of the normal (E_z) component of the electric field.

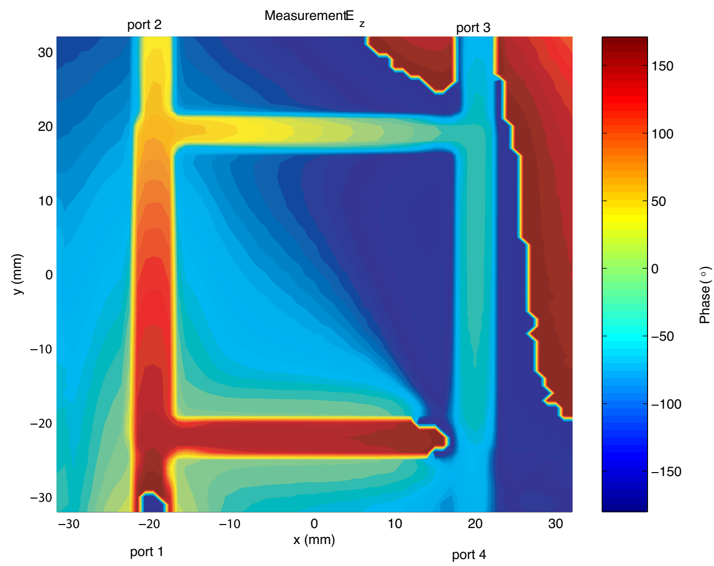

Figure 25. Phase measurement of the normal (E_z) component of the electric field.

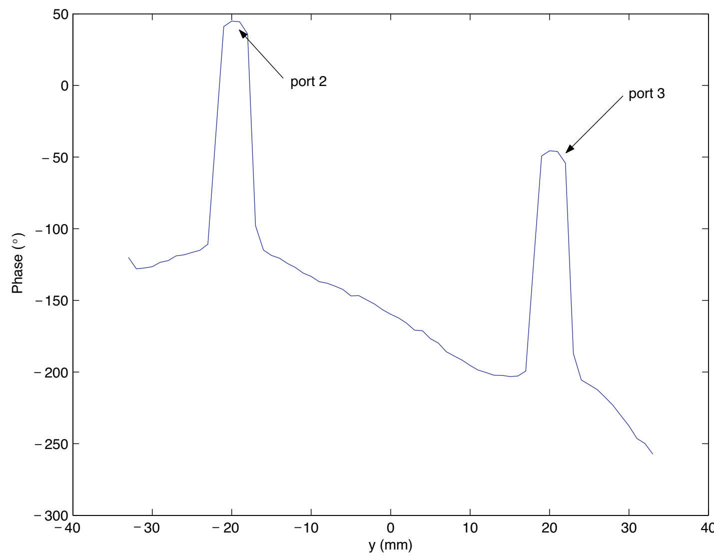

Figure 26. Cross section along y axis of phase measurement.

Phase measurements are coherent with a difference of 90° between port 2 and port 3. Measurements of this device show the ability of the test bench to produce amplitude and phase information of the normal component of the electric field with a good accuracy.

7. CONCLUSION

In this article we present a near-field test bench used to investigate EMI problems and in particular a study of the coaxial probe used to measure the normal component of the electric field. Parametric study of the probe shows that raising the length or the inner conductor diameter increases the sensibility. But for the first parameter, measured voltage corresponds to the integration of the electric field along the inner conductor extent. So, post processing is necessary to calculate the field in one point. For the second parameter, increasing the size of the probe also decreases the spatial resolution. Finally, a novel coaxial probe has been studied on micro-strip line in order to reduce coupling on external conductor because this coupling disturbs the electric field measurement. The probe's calibration on a wire over ground plane allows a simple and low cost procedure without using electromagnetic simulation to calculate radiated field. The near field test bench developed in our laboratory is used to locate emission sources of electronic systems in order to perform EMC investigations. These measurements can also be used for modeling the radiated emissions of components. A way explored in our laboratory is to design an equivalent model based on scalar potential calculated from electric measurements and on vector potential calculated from magnetic measurements. This model must be integrated in simulation platform to take into account EMC perturbations during the design of electronic systems.

REFERENCES

1. Haelvoet, K., S. Criel, F. Dobbelaere, L. Martens, P. De Laughe, and R. De Smedt, "Near-field scanner for the accurate characterization of electromagnetic fields in the close vicinity of electronic devices and systems," *IEEE Instrumentation and Measurement Technology Conference*, 1119–1122, Brussels, Belgium, June 1996.
2. Ostermann, T. and B. Deutschmann, "TEM-cell and surface scan to identify the electromagnetic emission of integrated circuits," *13th ACM Great Lakes Symposium on VLSI*, 76–79, Washington, USA, April 2003.

3. Tankielun, A., P. Kralicek, U. Keller, E. Sicard, and B. Vrignon, "Influence of core optimisation and activity for electromagnetic near-field and conducted emissions of CESAME test chip," *EMC Compo 2004 conference*, 95–100, Angers, France, April 2004.
4. Baudry, D., L. Bouchelouk, A. Louis, and B. Mazari, "Near-field test bench for complete characterization of components radiated emission," *EMC Compo 2004 Conference*, 85–89, Angers, France, April 2004.
5. Baudry, D., F. Bicrel, L. Bouchelouk, A. Louis, B. Mazari, and P. Eudeline, "Near-field techniques for detecting EMI sources," *IEEE Int. Symp. on EMC*, 11–13, Santa Clara, USA, August 2004.
6. Baudry, D., A. Louis, and B. Mazari, "A study and improvement of open-ended coaxial probe used for near-field measurements," *EMC Zurich Conference*, Zurich, Switzerland, February 2005.
7. Gao, Y. and I. Wolff, "Measurements of fields distributions and scattering parameters in multiconductor structures using an electric field probe," *IEEE MTT-S Int. Microw. Symp. Digest*, 1741–1744, Denver, USA, 1997.
8. Dutta, S. K., C. P. Vlahacos, D. E. Steinhauer, A. S. Thanawalla, B. J. Feenstra, F. C. Wellstood, and S. M. Anlage, "Imaging microwave electric fields using a near-field scanning microwave microscope," *Applied Physics Letters*, Vol. 74, No. 1, 156–158, January 1999.
9. Kazama, S. and K. I. Arai, "Adjacent electric field and magnetic field distribution," *IEEE Int. Symp. on EMC*, 395–400, Minneapolis, USA, 2002.
10. Laurin, J. J., Z. Ouardhiri, and J. Colinas, "Near-field imaging of radiated emission sources on printed-circuit boards," *IEEE Int. Symp. on EMC*, 368–373, Montreal, Canada, 2001.
11. Combes, P. F. and R. Crampagne, "Circuits passifs hyperfréquences: guides d'ondes métalliques," E 1401, traité Electronique, *Techniques de l'ingénieur*, 2002.
12. Dahele, J. S. and A. L. Cullen, "Electric probe measurements on microstrip," *IEEE Trans. Microw. Theory Tech.*, Vol. MTT-28, No. 7, 752–755, July 1980.
13. Baudry, D., "Conception, validation et exploitation d'un dispositif de mesure de champs électromagnétiques proches. Application CEM," *Thèse, Université de Rouen*, France, Avril 2005.